Performance of Detectors for Cooperative Spectrum Sensing Under Laplacian Noise

Luiz Gustavo Barros Guedes and Dayan Adionel Guimarães

***Abstract*—Electronic systems in general can be impaired by impulsive noise generated by a variety of sources. Spectrum sensors are of particular interest herein, since their probabilities of detection and false alarm can be severely degraded under this impairment. Several models for impulsive noise have been studied in the literature, all of them having the common characteristic of being well represented by heavy-tailed probability density functions, like Laplace and some Stable distributions. This article addresses the performances of state-of-the-art detectors for cooperative spectrum sensing when the received signal is impaired by Laplacian noise. This is made by means of estimating the probability of detection for a fixed false alarm rate, when important system parameters are varied. It is demonstrated that the robustness against impulsive noise varies significantly depending on the adopted detection strategy.**

***Index Terms*—Cognitive radio, cooperative spectrum sensing, dynamic spectrum access, impulsive noise, Laplacian noise.**

I. Introduction

With the unprecedented growing of wireless communication services working under a fixed bandwidth allocation policy, scarcity and underutilization of spectrum bands are experienced. The former consists of the dearth of new free bands, whereas the latter corresponds to the momentary unoccupation of some band by the primary user (PU), who owns the right to use of it.

A possible solution to the above-mentioned problems is the adoption of a dynamic spectrum access (DSA) policy, provided by secondary networks of cognitive radios, with the help of spectrum sensing [1]. The primary objective is to allow a flexible use of the spectrum bands among the PUs and the secondary users (SUs), which do not hold the priority right of using these bands [2]. These SUs should be able to seek for vacant bands, through spectrum sensing, for shared usage with the PUs.

Spectrum sensing is a binary hypothesis test in which the null hypothesis, $\mathcal{H}_0$, refers to the absence of the primary signal in the sensed band and the alternative hypothesis, $\mathcal{H}_1$, refers to the presence of the primary signal. By comparing a test statistic, T, with a decision threshold, γ, the test is performed. It is decided in favor of $\mathcal{H}_1$ if $T > \gamma$, or in favor of $\mathcal{H}_0$ otherwise. The purpose of this test is, therefore, to decide whether the received signal was generated under the hypothesis $\mathcal{H}_0$ or $\mathcal{H}_1$. There are two key performance metrics associated with this test: the probability of detection, P_{d}, and the probability of false alarm, P_{fa} [1]. The former is the probability of deciding that the PU signal is present in the sensed band, when it is indeed present, that is, $P_{\mathrm{d}} = P[T > \gamma|\mathcal{H}_1]$, while the latter is the probability of deciding that such a signal is present in the sensed band when, in fact, it is absent, that is, $P_{\mathrm{fa}} = P[T > \gamma|\mathcal{H}_0]$. Performance targets are, for example, $P_{\mathrm{d}} > 0.9$ and $P_{\mathrm{fa}} < 0.1$, as determined by the IEEE 802.22 standard [3].

Spectrum sensing can be made by a single SU, independently from the other SUs, which is referred to as non-cooperative spectrum sensing (NCSS), or can apply several SUs working together, which is referred to as cooperative spectrum sensing (CSS) [1]. Although multipath fading and signal shadowing degrade the performance of both NCSS and CSS, the degradation is less pronounced in the second case. This is because CSS takes advantage of the spatial diversity achieved with the use multiple SUs located in different positions.

In the centralized CSS with data fusion, which is the strategy adopted herein, the n samples collected by each of the m SUs in cooperation are transmitted to the fusion center (FC) belonging to the secondary network. Then, these samples are combined in order to allow for deciding upon the occupation state of the sensed band. In centralized CSS with decision fusion, local decisions made by each SU are sent to the FC, where these decisions are combined to form a global final decision about the occupancy state of the sensed channel [1].

In addition to the factors related to the signal propagation, it is well known that noise and different kinds of interference can degrade spectrum sensing performance. Regarding to the noise, its omnipresent form is the thermal noise or additive white Gaussian noise (AWGN), which is generated at the receiver side of every communication system. However, in specific environments, impulsive noise may be present either, and can be way more disastrous to the spectrum sensing performance than AWGN.

Impulsive noise [4] is an undesired random signal that contains occasional peaks of relatively high amplitude and short duration. Electromagnetic impulsive noise, which is considered in the present context, can originate from various sources, for instance:

- Switching devices: Switching devices such as relays, circuit breakers and switches can generate impulsive

Luiz G. B. Guedes and Dayan A. Guimarães, National Institute of Telecommunications (*Instituto Nacional de Telecomunicações*, Inatel), Santa Rita do Sapucaí - MG, e-mail: luizgustavo.barros@inatel.br, dayan@inatel.br, ORCID: 0000-0002-1823-4812, 0000-0002-1304-792X.

This work was partially supported by RNP, with resources from MCTIC, Grant 01245.020548/2021-07, under the Brazil 6G project of the Radiocommunication Reference Center (*Centro de Referência em Radiocomunicações* - CRR) of the National Institute of Telecommunications (*Instituto Nacional de Telecomunicações* - Inatel), Brazil, by Huawei, Grant PPA6001BRA23032110257684, under the project Advanced Academic Education in Telecommunications Networks and Systems, and by CNPq, Grant 302589/2021-0, Brazil. doi: 10.14209/jcis.2024.1.

noise when they open or close, which results from sudden changes in current flow;
- Lightning: Lightning discharges generate extremely high levels of impulsive electromagnetic noise due to the rapid discharge of electrical energy;
- Electric motors: Electric motors, especially those with brushes or commutators, can generate impulsive noise due to sparking and arcing within the motor. This noise can propagate through the power supply system or through electromagnetic radiation;
- Arcing and sparking: Electrical arcs and sparks, caused by loose connections, faulty wiring or damaged electrical equipment, produce impulsive noise. These sources are common in industrial environments, where high-power electrical equipment is used;
- Electrostatic discharge (ESD): ESD occurs when there is a sudden flow of static electricity between two objects with different potentials. It can generate impulsive noise that interferes with nearby electronic devices;
- Grounding issues: Poor grounding or inadequate shielding can lead to impulsive noise due to ground loops and unwanted electromagnetic coupling. These issues can result in noise pickup and interference in electronic systems.

When studying the influence of impulsive noise in electronic systems, the impulsive noise model can be selected from several ones available in the literature, such as: the Middleton Class A [4], the Gaussian mixture [5], the Bernoulli-Gaussian [4] and the symmetric alpha-stable (SαS) [4], [6]. The McLeish [7] distribution, also known as generalized symmetric Laplace or Bessel distribution, is also claimed to be suitable for modeling both Gaussian and non-Gaussian impulsive noise. The Middleton Class A model consists of a Poisson noise model form taking into account the impulse width in its probability density function (PDF). The Gaussian mixture model corresponds to a summation of a certain quantity of Gaussian components weighted according to the desired impulsiveness, allowing the adequate modeling of various classes of continuous models. The Bernoulli-Gaussian model corresponds to a Gaussian mixture based on the Bernoulli distribution, and the SαS model is a particularization of the α-stable (αS) distribution with adjacent samples temporarily uncorrelated.

In [8], it has been made an extensive study of the state-of-the-art regarding the interference models in communication systems, specially impulsive interference, departing from the studies by Middleton reported in [9].

It is easy to notice in the literature that the SαS distribution is typically adopted to characterize the heavy-tailed behavior of non-Gaussian noise, specially impulsive noise, in the CSS context, as can be seen for instance in [10]–[12]. For instance, in [13], the performance of a centralized CSS with data fusion is assessed, considering both SαS and alpha-sub-Gaussian (αSG) impulsive noise models. The latter keeps the amplitudes for each random variable following the SαS distribution, but introduces a non-zero temporal correlation among a group of adjacent samples.

A recent work has proposed the αSG [14], [15] distribution aiming to characterize both amplitude and temporal correlation among adjacent samples of the impulsive phenomena. The generalized Gaussian distribution was found to be suited for modeling not only the AWGN, but also non-Gaussian noises, such as impulsive noise, having as particularization the Laplace distribution [16]–[18].

The Laplacian noise model is considered in this article, aiming at evaluating its influence on a wide range of modern detectors for spectrum sensing. The Laplace distribution [18] is a member of the family of symmetric stable distributions, and is also known as the double-exponential distribution. It is characterized by heavy tails when compared to the Gaussian distribution, being often used to model data with outliers, which is the case of a signal corrupted by thermal plus impulsive noise [19]–[24].

A. Related research

Spectrum sensing with energy detection (ED) has been thoroughly analyzed in [25], considering a deterministic primary signal under AWGN. In [1], an adaptation of the ED test statistics has been derived, proving to be the optimal setting of this detection process in the aforementioned scenario. Although it is a relatively simple detection strategy in terms of implementation, the need to know the noise variance limits the operation of ED.

The absolute value cumulating (AVC) detector has been proposed in [26], where it is claimed that it is the most suitable technique for spectrum sensing under impulsive noise. Nonetheless, no justification about this attribute has been properly mentioned in the literature [22], [26], [27]. Indeed, the AVC is an optimal detector under Laplacian impulsive noise with fixed noise power and absence of fading, as demonstrated in the Appendix to this article.

The ED and the AVC are semi-blind detectors, since they require no information about the PU signal, but make use of the noise level information (respectively, the noise variance and its standard deviation) in their test statistic or to establish de decision threshold. The computational complexity of both ED and AVC is governed by the number of multiplications in the computation of the test statistic, when the noise variance or standard deviation is known a priori. However, in practice, the method applied to estimate the noise variance or standard deviation increases the overall computational complexities of ED and AVC beyond the complexities of many detectors, which is an aspect that is frequently disregarded in the literature.

The Gerschgorin radii and centers ratio (GRCR) detector, the Gini index detector (GID) and the Pietra-Ricci index detector (PRIDe) are innovative for cooperative or multi-antenna spectrum sensing. They have been proposed in [28], [29] and [30], respectively. These detectors are completely blind (requiring no information either on the PU signal and the noise level), have low computational complexity and attain robustness against variations or non-uniformity in the received signal and noise powers, allowing their performance metrics to remain practically unchanged in these scenarios. They also have the constant false alarm rate (CFAR) property, which

allows, for a target probability of false alarm, the establishment of the decision threshold independently of the noise variance. In addition, the GRCR, the GID and the PRIDe have similar or better performances compared to the most robust detectors present in the literature at the time of publication of [28], [29] and [30].

The GRCR, GID and PRIDe exhibit approximately the same computation complexity, which is low because their test statistics are formed by a direct operation on the elements of the received signal sample covariance matrix (SCM).

The locally most powerful invariant test (LMPIT) detector has been proposed in [31], and proved to be an attractive alternative for scenarios under low signal-to-noise ratio (SNR) regimes. Moreover, the LMPIT has low computation complexity, since its test statistic is formed by a direct operation on the elements of the SCM.

In [32] and [33], the Hadamard ratio (HR) detector and the volume-based detector number 1 (VD1) are addressed, respectively. In the former work, the authors have derived an expression for P_{d}, enabling a more accurate theoretical and numerical performance assessment for HR. In the latter, expressions for P_{d} and P_{fa} have been derived for the VD1. The computational complexity for the HR and VD1 is mainly governed by the computational cost associated to the formation of the SCM and in the calculation of its determinant.

In [34], the performance of two eigenvalue-based detectors for spectrum sensing is analyzed. The Roy's largest root test (RLRT) detector, also known as maximum eigenvalue detector (MED), requires precise knowledge of the noise variance, whereas the generalized likelihood ratio test (GLRT) detector does not. The authors have proposed expressions for P_{d} and P_{fa} in the case of the GLRT, as well as an expression of the difference in performance between such detectors, reaching the conclusion that accurate knowledge of noise variance can significantly increase detection capability, especially in scenarios with few sensors. The authors have also addressed the maximum-minimum eigenvalue detection (MMED) detector which, given its construction, is sub-optimal in comparison to the GLRT.

The arithmetic to geometric mean (AGM) detector has been proposed in [35]. It was conceived as an eigenvalue-based detector, established on the GLRT principle for spectrum sensing. Whether in the presence or absence of noise uncertainty, the AGM detector outperforms the ED given certain assumptions made by the authors regarding the primary signal. On the other hand, there is an increase in complexity due to the need to compute the SCM and estimate its eigenvalues.

The GLRT, the MMED and the AGM are blind detectors, since it is not necessary any information related to the primary signal neither the noise. The MED is semi-blind because it requires the noise variance information. The process of estimating the eigenvalues, which depends on the dimensions of the SCM, yields increased computational complexity and processing time for computing the test statistics of these detectors in comparison with the GRCR, GID, PRIDe and LMPIT.

B. Contributions and organization of the article

There are two fundamental contributions of this work:

1) The performance analysis of various state-of-the-art detectors for centralized CSS with data fusion when impaired by Laplacian noise is the main contribution. The detectors analyzed are: ED, AVC, GRCR, GID, PRIDe, LMPIT, HR, VD1, eigenvalue-based GLRT, MMED, MED and AGM. The performance comparisons are made by means of the probability of detection, for a CFAR of 0.1, as a function of the main CSS system parameters;
2) The demonstration (see the Appendix) of the optimality of the AVC detector when subjected to Laplacian impulsive noise, under the assumptions of fixed noise power and absence of fading, is also provided to fill a gap in the literature regarding such a demonstration.

The remaining of this article is structured as follows: Section II describes the system model adopted in the centralized CSS system, while Section III addresses the test statistics used in the performance analysis. Numerical results and discussions are given in Section IV. Section V concludes the work. As a complementary part of the article, the Appendix shows a detailed demonstration of the AVC's optimality when subjected to Laplacian noise.

II. System model

The signal model adopted herein refers to the centralized CSS with data fusion, wherein n samples proceeding from the primary signal, which has been transmitted by the PU, are collected by each of the m cooperating SUs and transmitted to the FC through an error-free control channel. At the FC, mn received samples compose the matrix $\mathbf{Y} \in \mathbb{R}^{m\times n}$, given by

$$\mathbf{Y} = \mathbf{h}\mathbf{x}^{\mathrm{T}} + (1-I)\mathbf{V} + I\mathbf{L}, \tag{1}$$

where I is an indicator variable such that $I = 1$ particularizes (1) for a sensing channel with Laplacian noise and $I = 0$ particularizes (1) for a pure AWGN channel. The vector $\mathbf{x} \in \mathbb{R}^{n\times 1}$, which models the PU signal, is composed of n real Gaussian samples with zero mean and variance defined according to the average SNR across the SUs. The use of samples following the Gaussian distribution is suitable for modeling the nature of envelope fluctuations of numerous modulated and filtered signals.

The channel vector $\mathbf{h} \in \mathbb{R}^{m\times 1}$ having elements h_i, $i = 1, 2, ..., m$, portraying the gains of the sensing channel between the PU and each SU, is given by

$$\mathbf{h} = \mathbf{G}\mathbf{a}, \tag{2}$$

where $\mathbf{a} \in \mathbb{R}^{m\times 1}$ is a vector assembled by real Gaussian random variables $a_i \sim \mathbb{R}\mathcal{N}[\sqrt{\kappa/(\kappa+1)}, 1/(\kappa+1)]$, where κ models the Rice factor [36] of the channel between the PU and the i-th SU. In dB, its value becomes $\kappa_{\mathrm{dB}} = 10\log_{10}(\kappa)$. The elements h_i are considered constants during each sensing interval and independent and identically distributed (iid) between successive sensing rounds. Furthermore, the bandwidth of the

primary signal is considered to be smaller than the coherence bandwidth of the sensing channel, which affects all frequency components of the signal in the same manner. In other words, this scenario corresponds to a flat fading channel.

According to [37], it has been verified that κ_{dB} is a random variable which depends on the environment where the associated system is inserted. It is modeled as a Gaussian random variable $\kappa_{\text{dB}} \sim \mathcal{N}[\mu_\kappa, \sigma_\kappa]$, considering both μ_κ and σ_κ in dB.

The matrix $\mathbf{G} \in \mathbb{R}^{m\times m}$ in (2) is given by

$$\mathbf{G} = \text{diag}\left(\sqrt{\frac{\mathbf{p}}{p_{\text{tx}}}}\right), \tag{3}$$

where $\mathbf{p} = [p_1 \ p_2 \ \cdots \ p_m]^{\text{T}}$ is the vector containing the received signal powers at the SUs, p_{tx} is the primary signal transmitted power, in watts, and $\text{diag}(\cdot)$ returns a diagonal matrix whose main diagonal is composed by the elements of the vector present in the argument.

The area-mean received power, p_i, by the i-th SU receiver at a given distance d_i from the PU transmitter can be calculated using the log-distance propagation prediction method [36] as

$$p_i = p_{\text{tx}}\left(\frac{d_0}{d_i}\right)^{\eta}, \tag{4}$$

where d_0 corresponds to a reference distance in the far-field region of the PU transmit antenna and η is the environment-dependent path-loss exponent [36]. The received power varies inversely proportional to the value of η at a given distance.

The elements in the i-th row of the matrix $\mathbf{V} \in \mathbb{R}^{m\times n}$, which models the AWGN noise, refer to the i-th SU and are iid Gaussian random variables, with zero mean and time-varying variance σ_i^2 given by

$${\sigma_i}^2 = (1 + \rho u_i)\sigma^2_{\text{avg}}, \tag{5}$$

where $0 \leq \rho < 1$ is the fractional variation of the noise power around its mean, $\sigma^2_{\text{avg}} = \frac{1}{m}\sum_{i=1}^{m}\sigma_i^2$, and u_i is the realization of a uniform random variable $\mathcal{U}_i \sim [-1, 1]$.

The instantaneous SNR, γ, across the SUs is given by

$$\gamma = \frac{1}{m}\sum_{i=1}^{m}\frac{p_i}{\sigma_i^2}. \tag{6}$$

Therefore, the average SNR across the SUs is given by

$$\text{SNR} = \mathbb{E}[\gamma], \tag{7}$$

where $\mathbb{E}[\cdot]$ returns the expected value of the random variable located into its argument. The final formula for the average SNR across the SUs, established in [38], whose details were omitted here for concision, is given by

$$\text{SNR} = \frac{\ln\left(\frac{1+\rho}{1-\rho}\right)}{2\rho m\sigma^2_{\text{avg}}}\sum_{i=1}^{m} p_i. \tag{8}$$

The matrix $\mathbf{L} \in \mathbb{R}^{m\times n}$ contains iid elements following the Laplace distribution, thus modeling the Laplacian noise samples. The Laplace (or double exponential) random variable [18, p. 16], l, with zero mean and variance equals to $2b^2$, presents its PDF as

$$f(l|b) = \frac{1}{2b}\exp\left(-\frac{l}{b}\right), \tag{9}$$

where $b > 0$ is the scale factor or diversity. Because the mean is fixed, the higher the value b is, the heavier the tail is.

III. Test statistics

Considering centralized CSS with data fusion, this section presents the test statistics of the detectors whose numerical results are compared in Section IV, namely: the ED, the AVC, the GRCR, the GID, the PRIDe, the LMPIT, the HR, the VD1, the GLRT, the MMED, the MED and the AGM.

The ED test statistic is given by [1]

$$T_{\text{ED}} = \sum_{i=1}^{m}\frac{1}{\sigma_i^2}\sum_{j=1}^{n}|y_{ij}|^2, \tag{10}$$

where σ_i^2 is the Gaussian noise variance at each SU and y_{ij} composes the matrix $\mathbf{Y}$ established in (1), referring to the j-th sample gathered by the i-th SU.

The test statistic of the AVC detector [26] is given by

$$T_{\text{AVC}} = \sum_{i=1}^{m}\frac{1}{\sigma_i}\sum_{j=1}^{n}|y_{ij}|, \tag{11}$$

where σ_i is the Gaussian noise standard deviation at each SU.

Among the above-mentioned detection criteria, some test statistics can be computed from the SCM of the received signal. It is formed at the FC and is given by

$$\hat{\mathbf{R}} = \frac{1}{n}\mathbf{Y}\mathbf{Y}^{\dagger}, \tag{12}$$

where $\dagger$ signifies the complex conjugate and transpose operation.

The test statistic of the GRCR [28] detector is given by

$$T_{\text{GRCR}} = \frac{\sum_{i=1}^{m}\sum_{j=1,j\neq i}^{m}|r_{ij}|}{\sum_{i=1}^{m} r_{ii}}, \tag{13}$$

where r_{ij} corresponds to the element in the i-th row and j-th column of $\hat{\mathbf{R}}$.

The test statistics of the GID [29] and PRIDe [30] detectors are given respectively by

$$T_{\text{GID}} = \frac{\sum_{i=1}^{m^2}|r_i|}{\sum_{i=1}^{m^2}\sum_{j=1}^{m^2}|r_i - r_j|} \tag{14}$$

and

$$T_{\text{PRIDe}} = \frac{\sum_{i=1}^{m^2}|r_i|}{\sum_{i=1}^{m^2}|r_i - \bar{r}|}, \tag{15}$$

where r_i is the i-th element of the vector $\mathbf{r}$ formed by stacking the columns of the SCM and $\bar{r} = (1/m^2)\sum_{i=1}^{m^2} r_i$.

For the LMPIT [31] detector, the test statistic is

$$T_{\text{LMPIT}} = \sum_{i=1}^{m}\sum_{j=1}^{m} |c_{ij}|^2, \tag{16}$$

where c_{ij} composes the i-th row and j-th column of the matrix $\mathbf{C} = \mathbf{E}^{-1/2}\hat{\mathbf{R}}\mathbf{E}^{-1/2}$. The diagonal matrix $\mathbf{E}$ presents elements equal to the main diagonal of $\hat{\mathbf{R}}$.

The test statistics of the HR [32] and VD1 [33] detectors are computed respectively by

$$T_{\text{HR}} = \frac{\det(\hat{\mathbf{R}})}{\prod_{i=1}^{m} r_{ii}} \tag{17}$$

and

$$T_{\text{VD1}} = \log[\det(\mathbf{S}^{-1}\hat{\mathbf{R}})], \tag{18}$$

where $\det(\cdot)$ denotes the determinant operation. The diagonal matrix $\mathbf{S}$ contains elements arranged in the vector $\mathbf{s} = [s_1 s_2 \cdots s_m]$, with $s_i = ||\hat{\mathbf{R}}(i,:)||_2$ and $||\cdot||_2$ denoting the Euclidean norm.

In the centralized eigenvalue-based CSS with data fusion, after calculating the SCM at the FC, its ordered eigenvalues ($\lambda_1 \geq \lambda_2 \geq \cdots \geq \lambda_m$) are estimated and the test statistics GLRT, MMED and MED can be built, respectively, as [34]

$$T_{\text{GLRT}} = \frac{\lambda_1}{\frac{1}{m}\sum_{i=1}^{m}\lambda_i}, \tag{19}$$

$$T_{\text{MMED}} = \frac{\lambda_1}{\lambda_m}, \tag{20}$$

$$T_{\text{MED}} = \frac{\lambda_1}{\sigma^2_{\text{avg}}}. \tag{21}$$

It is worth highlighting that the MED test statistic has been originally conceived considering equal noise variances across the SUs. However, in a practical scenario, the SUs are subjected to unequal and possibly time-varying noise variances, yielding performance loss for using the average noise power instead of the specific noise power levels in each SU, which, by the way, is not possible in (21).

For the AGM [35] detector, its test statistic is given by

$$T_{\text{AGM}} = \frac{\frac{1}{m}\sum_{i=1}^{m}\lambda_i}{(\prod_{i=1}^{m}\lambda_i)^{\frac{1}{m}}}. \tag{22}$$

IV. Numerical results

This section presents numerical results of the centralized CSS with data fusion. Systems in the absence and presence of impulsive noise, respectively, under Gaussian noise only and under Laplacian noise, are compared, for the detectors ED, AVC, GRCR, GID, PRIDe, LMPIT, HR, VD1, GLRT, MMED, MED and AGM.

The results expressed herein return the values of P_{d} achieved in accordance with the variation of the most relevant system parameters, assuming $P_{\text{fa}} = 0.1$ [3]. Each point on a curve has been generated from 10000 Monte Carlo events using the Matlab R2019a. In conformity with the methodology outlined in [39], a confidence interval analysis has been conducted using the binomial proportion confidence interval for a single proportion. This analysis has been made using the Matlab function `binofit`, which implements the Clopper-Pearson method [40]. The maximum confidence interval, corresponding to an estimated P_{d} equal to 0.5, was found to be 0.0197. This value clearly confers the level of accuracy suitable for the interpretation of the results presented herein. The Matlab code utilized to generate these results is available for retrieval from [41].

By making the absence of Laplacian noise scenario as reference, the value of the average SNR or the number of samples, n, has been adapted, in part of the cases, so that the respective best detector yields $P_{\text{d}} \approx 0.9$ at the mid-value of the system parameter being analyzed. Thus, variations in P_{d} can be clearly perceived. When fixed, for a better adequacy of situations more likely to occur in practice, the system configuration parameters are: $m = 6$ SUs, which corresponds to a small number of cooperative cognitive radios, leading to an efficient utilization of control channel resources. Additionally, the following curves show that an increase in the number of SUs results in a diminishing returns fashion of performance improvement; $n = 250$ samples to achieve the targeted performance metrics; SNR $= -10$ dB, considering that the system's operation may occur in scenarios characterized by significantly low SNR; fraction of noise variations, $\rho = 0.5$, which was arbitrarily chosen to model variations in thermal noise power due to changes in ambient temperature, some form of reception circuit descaling or interfering signals in the bandwidth of interest; path-loss exponent, $\eta = 2.5$, chosen to fit a typically urban scenario; normalized coverage radius, $r = 1$ m; reference distance for path-loss calculation, $d_0 = 0.001r$; $p_{\text{tx}} = 5$ W, adapting to practical requirements of power for real PU transmitters; and random Rice factor, with mean $\mu_\kappa = 1.88$ dB and standard deviation $\sigma_\kappa = 4.13$ dB, considering urban area [37]. The parameters related to the Laplacian noise have been calculated and generated as described in Section II.

Figs. 1 to 7 shows P_{d} as a function of the following system parameters: mean of Rice factor in dB, μ_κ; number of SUs in cooperation, m; path-loss exponent, η; number of samples collected per SU in each sensing round, n; average signal-to-noise ratio in dB over all SUs, SNR; fraction of noise power variations about the mean, ρ; and x-coordinate in m of the PU transmitter, equal to y-coordinate. In addition, such figures present one pair of graphs each (except for Fig. 6, which presents two pairs of graphs, explained more precisely in the following paragraphs). The graphs on the left show the performance assessment results under the absence of impulsive noise. The graphs on the right correspond to the performance results evaluated under Laplacian noise.

Prior to analyze the outcomes shown herein, it is noteworthy to know that a given detector does not have its performance affected in the same manner as another detector for the same system configuration and the same variation of a given parameter. This is justified because the received signal samples are handled by the test statistics differently from each other, which results in different behaviors among the detectors.

Fig. 1 gives P_{d} versus mean of Rice factor, μ_κ, in dB. In the absence (left-hand side graph) and in the presence (right-hand

side graph) of Laplacian noise, it can be seen that the mean of Rice factor has a certain influence on the performance of the various detectors just from around $\mu_\kappa \approx -5$ dB. This value corresponds to a situation in which the dominant component of the primary signal starts to stand out in relation to the scattered component, thus increasing the performance of most detectors, in different proportions. For mean of Rice factor values greater than 5 dB, the detectors GID, PRIDe, ED, AVC, HR, VD1, GRCR and LMPIT tend to show similar and optimal performances. The exception is found in the performance drop shown by the ED in the presence of Laplacian noise. The MMED and the AGM detectors showed the worst performance for any values of μ_κ in both scenarios.

Fig. 1a, referring to the absence of Laplacian noise, shows ED outperforming the other detectors, as expected, and followed by the AVC detector. It can be seen that the LMPIT, the GRCR, the HR and the VD1 detectors present similar performances for any mean of Rice factor values. The PRIDe and the MED detectors have analogous performances for lower values of μ_κ, with the former outperforming the latter from $\mu_\kappa \approx -5$ dB. The GLRT has the worst performance, followed, respectively, by the MMED and by the AGM, whose curves remain practically invariable with the change in the parameter μ_κ. For smaller values of μ_κ, the GID show the worst performance, but, for higher values of the mean of Rice factor, its performance improve significantly, with its curve tending to the optimal ones of the PRIDe, the HR, the VD1, the GRCR, the ED, the LMPIT and the AVC detectors. There is not an specific reason for this behavior. It is a feature of the detector itself, present in the following results either, that causes it to react differently in relation to other detectors to the variation of the same parameter.

From Fig. 1b, it is noticed that there is a maintenance in the pattern of the curves, only with a performance reduction for most of the detectors due to the presence of Laplacian noise, in comparison to the absence of Laplacian noise scenario. The exception is for the AVC detector, which presents a performance improvement and excels the other detectors for all values of μ_κ. A more evident deterioration in the performance of the ED, the MED, the GLRT and the MMED detectors can be seen, in relation to the other detectors, when compared with the scenario of absence of Laplacian noise. It can be noticed a great robustness against Laplacian noise for the GID, the PRIDe, the HR, the VD1, the GRCR and the LMPIT detectors, which have presented performance curves tending to be very similar to those achieved in the scenario that disregards the presence of impulsive noise.

Fig. 2 shows P_d versus number of SUs in cooperation, m. It can be seen that there is an improvement in the performance of all detectors with an increase in the value of m, either in the absence (left-hand side graph) or in the presence (right-hand side graph) of Laplacian noise. Due to the increase in the number of SUs in cooperation, there is an increase in spatial diversity gain, with consequent performance improvement. The pattern of the curves is maintained in both scenarios, emphasizing the more severe performance loss suffered by the ED and the MED detectors in the presence of Laplacian noise. A notable performance improvement of the AVC detector in this scenario is also observed.

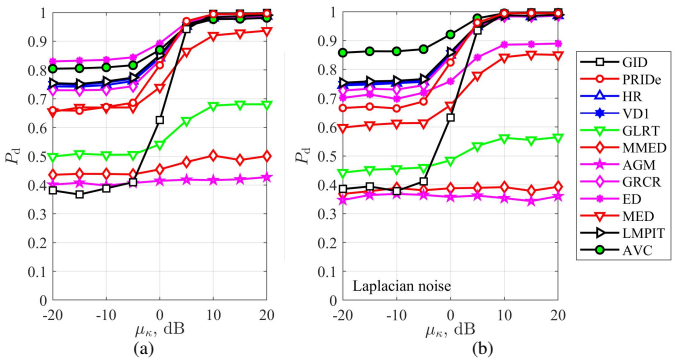

Fig. 1. Probability of detection, P_d, versus mean of Rice factor (dB), μ_κ, for SNR $= -$ 8 dB: system under Gaussian noise (left) and system under Laplacian noise (right). This figure is better viewed in color.

When the system is under Gaussian noise only, as shown in Fig. 2a, the ED performs slightly better than the AVC and more prominently compared to other detectors, for any value of m. The PRIDe, the HR, the VD1, the GRCR and the LMPIT detectors have a similar performance curve along all values of m in use, being inferior to the ED and the AVC for smaller values of m, but having similar performances to both for larger values of this same system parameter. The GID and the MED show similar performances, lower than those of the aforementioned detectors. The GLRT, the MMED and the AGM detectors return the worst performances for any values of m, with the first one outperforming the second one and the AGM.

From Fig. 2b, it is seen that, when the system is subjected to Laplacian noise, there is a significant performance loss for the ED and a meaningful robustness against this type of noise for the AVC detector. Mainly the PRIDe, followed by the HR, the VD1, the GRCR and the LMPIT detectors have a great robustness in this scenario, unlike the MED, the GLRT, the AGM and the MMED, whose performances were degraded by the presence of Laplacian noise. It is noteworthy to mention that the GID, the PRIDe, the HR, the VD1, the GRCR and the LMPIT do not have their performances affected by the presence of impulsive noise. All comparisons made here take, as reference, the absence of impulsive noise situation.

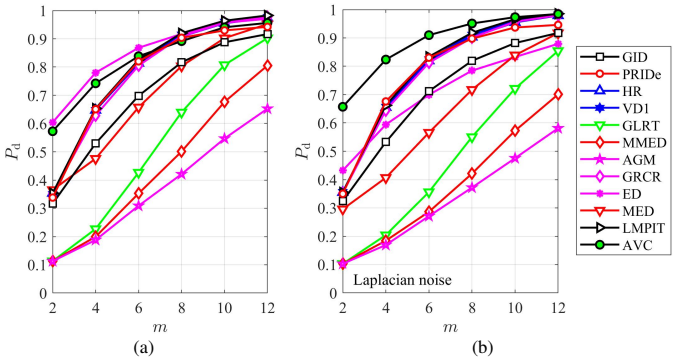

Fig. 2. Probability of detection, P_d, versus number of SUs in cooperation, m, for SNR $= -$ 9 dB: system under Gaussian noise (left) and system under Laplacian noise (right). This figure is better viewed in color.

Fig. 3 shows P_{d} versus path-loss exponent, η. No performance improvement is observed with the variation of this parameter for the different detectors. Either there is performance maintenance, or there is a reduction. The path-loss exponent indicates how the received signal power decays with distance. The higher its value, the more intense the signal power tends to drop with distance. In both scenarios, a more pronounced drop in the performance of the GID, the PRIDe, the HR, the VD1, the GRCR and the LMPIT detectors is noticed with the increase in the value of the path-loss exponent, whereas, for the other detectors, there is a certain constancy or slight drop in performance with the variation of η.

As expected, from Fig. 3a, the ED outperforms the other detectors, followed by the AVC detector. Its curves are slightly penalized with the increase in the value of η. The PRIDe, the HR, the VD1, the GRCR and the LMPIT detectors present very similar performance curves, being more compromised as the value of the path-loss exponent increases. This same behavior can be seen in the performance of the GID detector, whose curve is little below from the aforementioned detectors. The MED and GLRT performance curves are discreetly penalized as the path-loss exponent value increases, with the former surpassing the GID curve only for $\eta \geq 3$ and with the latter showing the worst values of P_{d} for any values of η. The MMED and the AGM detectors return the worst performers regardless of the value of η.

From Fig. 3b, it is noticed a maintenance in the pattern of the curves, compared to the Fig. 3a, except for the severe sensitivity to the presence of impulsive noise suffered by the ED, the MED, the GLRT, the MMED and the AGM detectors. In this scenario, there is no path-loss exponent value that causes the MED curve to be above the GID curve. Once again, the GID, the PRIDe, the HR, the VD1, the GRCR and the LMPIT do not have any performance change in the presence of the Laplacian noise, in relation to the absence of this type of noise. The robustness of the AVC to the presence of Laplacian noise is so evident that its performance improves, in relation to the scenario without impulsive noise, and surpasses the other detectors, for any values of η.

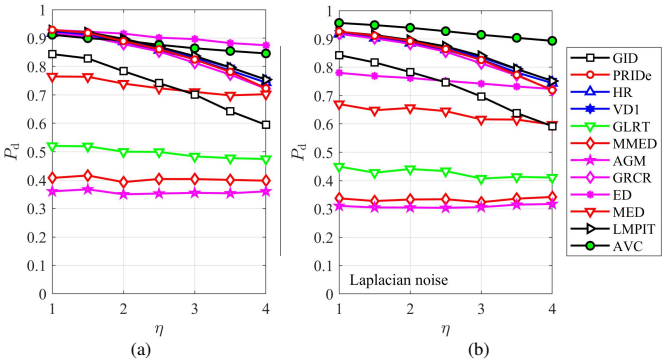

Fig. 3. Probability of detection, P_{d}, versus path-loss exponent, η, for SNR $= -8.5$ dB: system under Gaussian noise (left) and system under Laplacian noise (right). This figure is better viewed in color.

Fig. 4 shows P_{d} versus number of samples collected per SU in each sensing round, n. The accuracy in deciding on the state of occupancy of the user's band holding the right of use is higher when a greater number of samples are gathered in a given sensing interval, keeping the sampling rate fixed. This is why the performance of all detectors improves with the variation in the value of n. It can be seen a poor performance for the GLRT, the MMED and the AGM in both scenarios. There is a steep improvement in the performance of the various detectors up to $n = 400$ samples. From this value, the improvement becomes smoother.

Fig. 4a shows the ED outperforming the other detectors, followed by the AVC detector. Once again, the PRIDe, the HR, the VD1, the GRCR and the LMPIT detectors have similar performances. For larger values of n, their performances tend to overlap with each other and with those of the ED and the AVC detectors. With a little worse performances than those above-mentioned, we have, again, the GID followed by the MED. Note that the performances of the MED, the GLRT, the MMED and the AGM tend to remain constant from $n = 400$.

From Fig. 4b, it can be seen the same pattern of the curves, compared to the Fig. 4a, except, once again, for the strict sensitivity to the presence of Laplacian noise suffered by the ED, the MED, the GLRT, the MMED and the AGM detectors. The ED curve was affected in such a way as to be between the GID and the MED curves. On the other hand, the AVC detector considerably outperformed other detectors in the presence of impulsive noise, for any value of n. Once again, the GID, the PRIDe, the HR, the VD1, the GRCR and the LMPIT do not have any performance change in the presence of the Laplacian noise, in relation to the absence of this kind of noise.

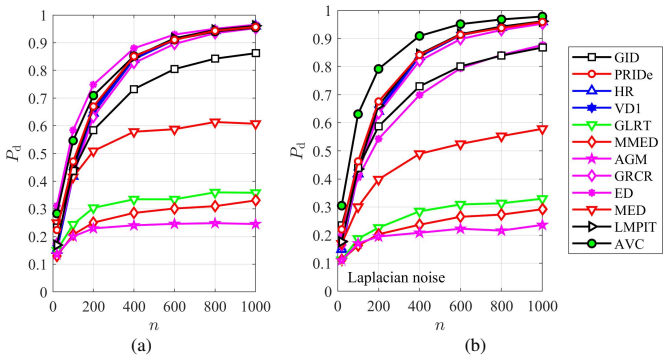

Fig. 4. Probability of detection, P_{d}, versus number of samples collected per SU in each sensing round, n, for SNR $= -10$ dB: system under Gaussian noise (left) and system under Laplacian noise (right). This figure is better viewed in color.

Fig. 5 shows P_{d} versus average signal-to-noise ratio over all SUs, SNR in dB. As expected, the results show an increase in the performance of all detectors with the SNR. Again, it can be noticed that the GLRT, the MMED and the AGM detectors have the worst performances in both scenarios and for any value of SNR.

As shown in Figs. 1a to 4a, Fig. 5a presents the ED standing out the other detectors, as expected. Then, it is followed by the AVC detector. Afresh, the PRIDe, the HR, the VD1, the GRCR and the LMPIT detectors have similar performances, with the former mildly outperforming the other ones. For SNR > -7.5 dB, their curves tend to overlap and to get optimal performances, along with those of the ED and the AVC detectors. For most SNR values, the MED, the

GLRT, the MMED and the AGM detectors present the worst performances. An interesting point is that the GID outperform the PRIDe, for lower SNR values (up to about -15 dB), being below only the ED and the AVC detectors in this case. From this value onwards, its curve is below that of the others above-mentioned. For SNR > -7.5 dB, it tends to be overcome even by the MED, the GLRT, the MMED and the AGM detectors.

From Fig. 5b, it is observed that the AVC detector stands out the other detectors in the presence of Laplacian noise. The ED, the MED, the GLRT, the MMED and the AGM detectors have their performances affected by the presence of this type of noise, perceiving a more significant sensitivity for the ED than for the other detectors. The GID, the PRIDe, the HR, the VD1, the GRCR and the LMPIT detectors show a visible robustness to the Laplacian noise, since their curves have kept the pattern observed in the absence of Laplacian noise scenario, which has been taken as reference.

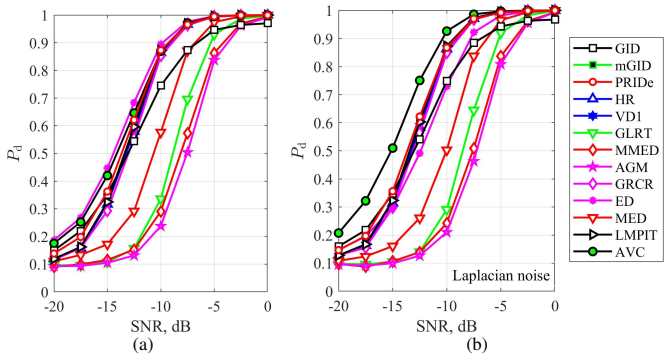

Fig. 5. Probability of detection, P_{d}, versus average signal-to-noise ratio over all SUs, SNR in dB, for $n = 450$: system under Gaussian noise (left) and system under Laplacian noise (right). This figure is better viewed in color.

Fig. 6 presents P_{d} versus fraction of noise power variations about the mean, ρ. The graphs reveal that the performance of all detectors, although in different proportions, tends to worsen as the value of ρ increases. The noise uncertainty can be interpreted as a certain inaccuracy in the process of estimating the variance or the standard deviation of noise when it is necessary to use them in computing test statistic and these parameters are unknown. Another possible perspective refers to the assumption that variations in the real variance values may occur due to two main reasons, even if the estimated variance is properly established during the detector design phase: unwanted signals being captured by the receiver and irregular calibration on the receiver's front-end.

From Fig. 6a, considering the absence of Laplacian noise and noise uncertainty not applied, it can be seen that the ED tends to surpass the other detectors, except for lower values of ρ, when the MED and the GLRT detectors tend to return better performances. For the AVC, the LMPIT, the PRIDe, the HR, the VD1 and the GRCR detectors, it is verified similar behaviors. Until $\rho = 0.4$, its curves remain invariables. From this value, these detectors show a slight drop in performance. The GID detector presents a lower performance than these detectors. The MED, the GLRT, the MMED and the AGM show a more abrupt drop in performance, particularly from $\rho = 0.2$.

Maintaining the non-application of noise uncertainty, but inserting the system in a scenario with the presence of Laplacian noise, as seen in Fig. 6b, it can be noticed that the pattern of the curves is maintained, taking the absence of Laplacian noise as reference. The AVC detector outperforms other detectors for any values of ρ. The ED suffers a severe loss of performance, with its curve positioned very close to that of the GID. The MED, the GLRT, the MMED and the AGM suffered a minor performance loss in this scenario, compared to the ED curve. The GID, the PRIDe, the HR, the VD1, the GRCR and the LMPIT detectors, once again, show an evident robustness against Laplacian noise, as their performances have kept the same pattern analyzed in the absence of impulsive noise scenario.

Figs. 6c and 6d unveil the application of noise uncertainty in the absence (left-hand graph) and in the presence (right-hand graph) of Laplacian noise. The pattern of the curves are kept from the previous scenario, except for the ED and the AVC. Detectors that are influenced by noise uncertainty present either the variance or the standard deviation when calculating their test statistics. Therefore, the influence on the ED, the AVC and the MED detectors is noticeable. In the absence of Laplacian noise, the ED and the AVC exhibit severe performance degradation. A greater robustness of the MED is noted when considering the noise uncertainty, as its performance is slightly degraded, surpassing even the AVC detector one. It is worth remembering that both comparisons were made with the situation without impulsive noise and without applying noise uncertainty. It is interesting to note that the optimal condition of the AVC detector under Laplacian noise is lost when considering noise uncertainty.

Finally, Fig. 7 show P_{d} versus x-coordinate of the PU transmitter in meters, m, equal to y-coordinate. For values of $x = y < 3r$, it is noted that the more robust detectors present a decreased performance, in different proportions, when compared with them even from this coordinate value of the PU transmitter, in which one can see, for all detectors, an invariability in the value of P_{d}. The first case is due to greater relative differences among the received signal powers, which is equivalent to an increase in the value of the path-loss exponent. The second case means that there is insignificant relative differences among the received signal powers, not causing, therefore, improvement or loss of performance. From the other analyzes covered in this work, it appears that there is a pattern in the performances of detectors that are more robust and those that are more sensitive, whether in the scenario considering absence (left-hand side graph) and presence (right-hand side graph) of Laplacian noise. Once again, the superiority of the AVC detector, compared to other detectors, in the presence of impulsive noise, stands out.

V. Conclusions

This work has assessed the performance of centralized cooperative spectrum sensing with data fusion, under Laplacian impulsive noise. The performances of the detectors ED, AVC, GRCR, GID, PRIDe, LMPIT, HR, VD1, GLRT, MMED, MED and AGM were compared under Gaussian noise and under Laplacian noise models.

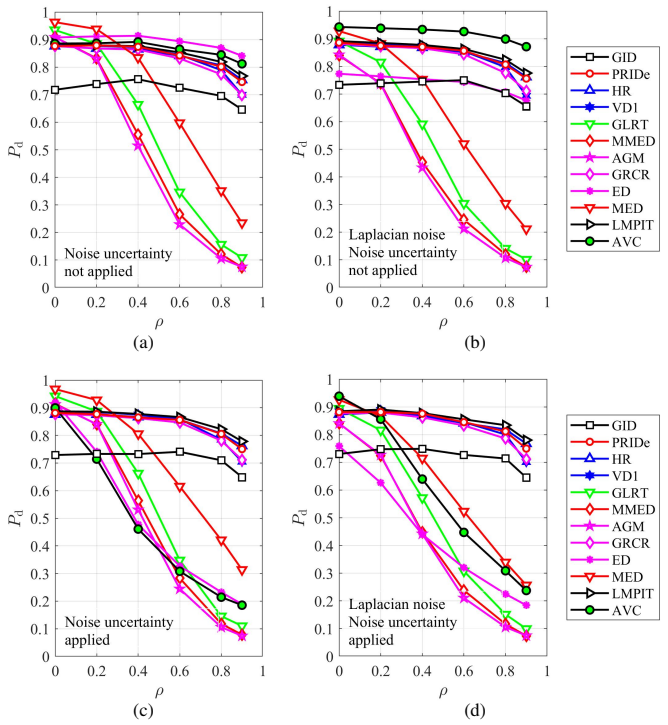

Fig. 6. Probability of detection, $P_{\rm d}$, versus fraction of noise power variations about the mean, ρ, for SNR $= -$ 8.5 dB: system under Gaussian noise (left) and system under Laplacian noise (right). Noise uncertainty not applied (above) and applied (below). This figure is better viewed in color.

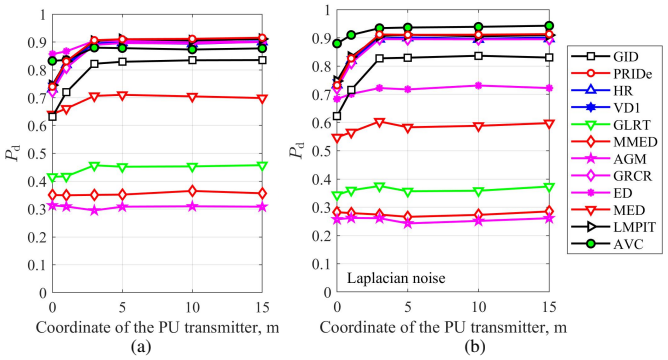

Fig. 7. Probability of detection, $P_{\rm d}$, versus x-coordinate of the PU transmitter, m, equal to y-coordinate, for SNR $= -$ 9 dB: system under Gaussian noise (left) and system under Laplacian noise (right). This figure is better viewed in color.

The AVC detector has shown excellent performance under Laplacian noise, but, from what was concluded in the Appendix, it will no longer be optimal under other types of noise. For any values of the analyzed parameters, it can be noted a great robustness for the AVC detector in the presence of Laplacian noise, since there was an outperforming pattern, in comparison with the other detectors.

It has been verified either that the GID, the PRIDe, the HR, the VD1, the GRCR and the LMPIT detectors do not have any performance modification in the presence of the Laplacian noise, in relation to the absence of this type of noise. This indicates the significant robustness of such detectors and, therefore, their suitability against the potential degrading effects imposed by the Laplacian noise. On the other hand, the ED, the MED, the GLRT, the MMED and the AGM detectors have demonstrated a significant sensibility against the Laplacian impulsive noise, especially the ED, which went from a reference behavior, in the absence of impulsive noise, to an intermediate behavior, in the presence of the Laplacian noise. For that reason, the use of these latter detectors proved to be inappropriate for spectrum sensing under Laplacian impulsive noise, in contrast with the former ones.

As an opportunity for contribution in future researches, this performance analysis can be extended to other types of impulsive noise. It becomes interesting either to develop or improve a given detector in order to make it optimal or even more robust for any type of impulsive noise. Another opportunity that can be considered is the assessment of the detectors' performances under impulsive noise, but considering other channel fading models, or even other impulsive noise models.

APPENDIX

The paramount claiming in the design of a detector is to establish a test statistic T and set the decision threshold γ in order to achieve a targeted spectrum sensing performance. For this purpose, it is going to be used the classical approach, represented here by the Neyman-Pearson criterion, which has as main objective finding T and γ so the probability of detection is maximized under a restriction on the maximum probability of false alarm.

A test statistic given as a result of the Neyman-Pearson criterion can be formed as a ratio of two quantities or a scaling factor of it and rewritten as follows, named as log-likelihood ratio (LLR) [1]

$$T = \log\left[\frac{p(\mathbf{y}|\mathcal{H}_1)}{p(\mathbf{y}|\mathcal{H}_0)}\right], \tag{23}$$

where $p(\mathbf{y}|\mathcal{H}_1)$ and $p(\mathbf{y}|\mathcal{H}_0)$ refer to PDFs of the n-dimensional received signal vector $\mathbf{y}$, respectively conditioned on the hypotheses $\mathcal{H}_1$ and $\mathcal{H}_0$.

Let's consider that the vector $\mathbf{y}$ containing n signal samples plus noise is received by an SU, so that,

$$\mathbf{y} = \mathbf{x} + \mathbf{v}, \tag{24}$$

where $\mathbf{x}$ and $\mathbf{v}$ correspond to the vectors which contains, respectively, the primary signal and the noise samples present at the SU.

It is assumed that $\mathbf{v}$ is a vector of iid complex Laplace [42] random variables with zero mean and variance σ^2, that is, $\mathbf{v}$ $\mathbb{CL}[\mathbf{0}, \sigma^2\mathbf{I}]$, where $\mathbf{I}$ is the identity matrix of order $n \times n$ and $\sigma^2\mathbf{I}$ corresponds to the covariance matrix of $\mathbf{v}$. Thus, it follows that $\mathbf{y} = \mathbf{v}$, under the hypothesis $\mathcal{H}_0$, and $\mathbf{y} = \mathbf{x} + \mathbf{v}$, under the hypothesis $\mathcal{H}_1$.

It is assumed that $\mathbf{y}$ does not have any arrangement that can be exploited to ease the detection process. In this case, it is addressed that $\mathbf{x}$ is simply a vector of iid complex Laplace random variables with zero mean and variance σ_X^2, that is, $\mathbf{y}$ $\mathbb{CL}[\mathbf{0}, \sigma^2\mathbf{I}]$, under $\mathcal{H}_0$, and $\mathbf{y}$ $\mathbb{CL}[\mathbf{0}, (\sigma^2 + \sigma_X^2)\mathbf{I}]$ under $\mathcal{H}_1$.

It is known that the PDF of an n-dimensional random vector $\mathbf{z}$ having real Laplace-distributed entries, mean $\mu = 0$ and covariance matrix $\mathbf{\Sigma}$ is given by [43]

$$\begin{aligned} p(\mathbf{z}) &= p(z_1, z_2, ..., z_n) \\ &= \frac{2}{(2\pi)^{v+1}\det(\mathbf{\Sigma})^{\frac{1}{2}}} \times \frac{\mathcal{K}_v(\sqrt{2\mathbf{z}^{\mathrm{T}}\Sigma^{-1}\mathbf{z}})}{(\sqrt{\mathbf{z}^{\mathrm{T}}\Sigma^{-1}\mathbf{z}/2})^v}, \end{aligned} \tag{25}$$

where $p(\mathbf{z}) = p(z_1, z_2, ..., z_n)$ denotes the joint PDF of the elements of $\mathbf{z}$, $v = \frac{n}{2} - 1$ and $\mathcal{K}_v(\cdot)$ is the modified Bessel function of the second kind with order v. An well known asymptotic formula for this Bessel function is given as follows [43]

$$\mathcal{K}_v(d) \approx \sqrt{\frac{\pi}{2d}}\exp(-d), \tag{26}$$

while $|d|$ tends to infinity. Using $d = \sqrt{2\mathbf{z}^{\mathrm{T}}\Sigma^{-1}\mathbf{z}}$, it follows that

$$\begin{aligned} \mathcal{K}_{\frac{n}{2}-1}(\sqrt{2\mathbf{z}^{\mathrm{T}}\Sigma^{-1}\mathbf{z}}) &= \sqrt{\frac{\pi}{2\sqrt{2\mathbf{z}^{\mathrm{T}}\Sigma^{-1}\mathbf{z}}}}\exp(-\sqrt{2\mathbf{z}^{\mathrm{T}}\Sigma^{-1}\mathbf{z}}) \\ &= \left(\frac{\pi}{2\sqrt{2\mathbf{z}^{\mathrm{T}}\Sigma^{-1}\mathbf{z}}}\right)^{\frac{1}{2}} \exp(-\sqrt{2\mathbf{z}^{\mathrm{T}}\Sigma^{-1}\mathbf{z}}). \end{aligned} \tag{27}$$

Applying (27) into (25), we succeed in the final formula for the joint PDF of the elements of $\mathbf{z}$, $p(\mathbf{z})$, in the subsequent manner

$$p(\mathbf{z}) = \frac{2}{(2\pi)^{\frac{n}{2}}\det(\mathbf{\Sigma})^{\frac{1}{2}}} \times \frac{\left(\frac{\pi}{2\sqrt{2\mathbf{z}^{\mathrm{T}}\Sigma^{-1}\mathbf{z}}}\right)^{\frac{1}{2}} \exp(-\sqrt{2\mathbf{z}^{\mathrm{T}}\Sigma^{-1}\mathbf{z}})}{(\sqrt{\mathbf{z}^{\mathrm{T}}\Sigma^{-1}\mathbf{z}/2})^{\frac{n}{2}-1}}. \tag{28}$$

Solving separately for each hypothesis, initiating by $p(\mathbf{y}|\mathcal{H}_1)$, it follows that

$$\begin{aligned} p(\mathbf{y}|\mathcal{H}_1) = & \\ & \frac{2}{(2\pi)^{\frac{n}{2}}(\sigma^2+\sigma_X^2)^{\frac{1}{2}}} \\ & \times \frac{\left(\frac{\pi}{2\sqrt{2||\mathbf{y}||^2\Sigma^{-1}}}\right)^{\frac{1}{2}} \exp(-\sqrt{2||\mathbf{y}||^2\Sigma^{-1}})}{(\sqrt{||\mathbf{y}||^2\Sigma^{-1}/2})^{\frac{n}{2}-1}} \\ & = \frac{2}{(2\pi)^{\frac{n}{2}}(\sigma^2+\sigma_X^2)^{\frac{1}{2}}} \\ & \times \frac{\left(\frac{\pi}{2\sqrt{2\frac{||\mathbf{y}||^2}{\sigma^2+\sigma_X^2}}}\right)^{\frac{1}{2}} \exp\left(-\sqrt{2\frac{||\mathbf{y}||^2}{\sigma^2+\sigma_X^2}}\right)}{\left(\sqrt{\frac{||\mathbf{y}||^2}{2(\sigma^2+\sigma_X^2)}}\right)^{\frac{n}{2}-1}} \\ & = \frac{2}{(2\pi)^{\frac{n}{2}}(\sigma^2+\sigma_X^2)^{\frac{1}{2}}} \\ & \times \frac{\frac{\pi^{\frac{1}{2}}}{\left(\frac{2\sqrt{2}||\mathbf{y}||}{(\sigma^2+\sigma_X^2)^{\frac{1}{2}}}\right)^{\frac{1}{2}}} \exp\left(-\frac{\sqrt{2}||\mathbf{y}||}{(\sigma^2+\sigma_X^2)^{\frac{1}{2}}}\right)}{\left(\frac{||\mathbf{y}||}{\sqrt{2}(\sigma^2+\sigma_X^2)^{\frac{1}{2}}}\right)^{\frac{n}{2}-1}} \\ & = \frac{2(\pi(\sigma^2+\sigma_X^2)^{\frac{1}{2}})^{\frac{1}{2}}(\sqrt{2}(\sigma^2+\sigma_X^2)^{\frac{1}{2}})^{\frac{n}{2}-1}}{(2\pi)^{\frac{n}{2}}(\sigma^2+\sigma_X^2)^{\frac{1}{2}}(2\sqrt{2})^{\frac{1}{2}}} \\ & \times \frac{1}{||\mathbf{y}||^{\frac{n}{2}-\frac{1}{2}}} \exp\left(-\frac{\sqrt{2}||\mathbf{y}||}{(\sigma^2+\sigma_X^2)^{\frac{1}{2}}}\right). \end{aligned} \tag{29}$$

Using the same strategy in order to calculate $p(\mathbf{y}|\mathcal{H}_0)$, we have

$$\begin{aligned} p(\mathbf{y}|\mathcal{H}_0) = & \\ & \frac{2}{(2\pi)^{\frac{n}{2}}(\sigma^2)^{\frac{1}{2}}} \\ & \times \frac{\left(\frac{\pi}{2\sqrt{2||\mathbf{y}||^2\Sigma^{-1}}}\right)^{\frac{1}{2}} \exp(-\sqrt{2||\mathbf{y}||^2\Sigma^{-1}})}{(\sqrt{||\mathbf{y}||^2\Sigma^{-1}/2})^{\frac{n}{2}-1}} \\ & = \frac{2}{(2\pi)^{\frac{n}{2}}\sigma} \\ & \times \frac{\left(\frac{\pi}{2\sqrt{2\frac{||\mathbf{y}||^2}{\sigma^2}}}\right)^{\frac{1}{2}} \exp\left(-\sqrt{2\frac{||\mathbf{y}||^2}{\sigma^2}}\right)}{\left(\sqrt{\frac{||\mathbf{y}||^2}{2\sigma^2}}\right)^{\frac{n}{2}-1}} \\ & = \frac{2(\pi\sigma)^{\frac{1}{2}}(\sqrt{2}\sigma)^{\frac{n}{2}-1}}{(2\pi)^{\frac{n}{2}}\sigma(2\sqrt{2})^{\frac{1}{2}}} \\ & \times \frac{1}{||\mathbf{y}||^{\frac{n}{2}-\frac{1}{2}}} \exp\left(-\frac{\sqrt{2}||\mathbf{y}||}{\sigma}\right). \end{aligned} \tag{30}$$

Every term that is independent of $\mathbf{y}$ can be considered as a proportionality constant which does not interfer in the final result of the test statistic. Applying this consideration and overwriting both (30) and (29) in (23), then

$$\begin{aligned} T &\propto \ln\left[\frac{\frac{1}{||\mathbf{y}||^{\frac{n}{2}-\frac{1}{2}}}\exp\left(-\frac{\sqrt{2}||\mathbf{y}||}{(\sigma^2+\sigma_X^2)^{\frac{1}{2}}}\right)}{\frac{1}{||\mathbf{y}||^{\frac{n}{2}-\frac{1}{2}}}\exp\left(-\frac{\sqrt{2}||\mathbf{y}||}{\sigma}\right)}\right] \\ &\propto \ln\left[\frac{\exp\left(-\frac{\sqrt{2}||\mathbf{y}||}{(\sigma^2+\sigma_X^2)^{\frac{1}{2}}}\right)}{\exp\left(-\frac{\sqrt{2}||\mathbf{y}||}{\sigma}\right)}\right]. \end{aligned} \tag{31}$$

Applying $\ln(a/b) = \ln(a) - \ln(b)$, it follows that

$$T \propto \left(-\frac{\sqrt{2}}{(\sigma^2+\sigma_X^2)^{\frac{1}{2}}} + \frac{\sqrt{2}}{\sigma}\right)||\mathbf{y}||, \tag{32}$$

meaning that the resulting test statistic is proportional to $||\mathbf{y}||$. Once again, since the proportionality constant is independent of $\mathbf{y}$, then

$$\begin{aligned} T &\propto ||\mathbf{y}|| \\ &= \sqrt{\mathbf{y}^{\mathrm{T}}\mathbf{y}} \\ &= \sum_{i=1}^{n}\sqrt{y_i^* y_i} \\ &= \sum_{i=1}^{n}\sqrt{|y_i|^2} \end{aligned}$$

$$= \sum_{i=1}^{n} |y_i|. \tag{33}$$

The performance of the hypothesis test is not affected by any proportionality constant assigned to the test statistic formula, because its decision threshold is changed in the same proportion. Therefore, it has been assigned the $1/n$ proportionality constant to (33) just for convenience herein,

$$T_{\mathrm{AVC}} = \frac{1}{n} \sum_{i=1}^{n} |y_i|. \tag{34}$$

The test statistic from (33) or (34) corresponds to the absolute value cumulating (AVC) detector, which has been shown as an optimal detector, according to the Neyman-Pearson criterion, under the conditions assigned by the signal model stated in the present appendix.

REFERENCES

[1] D. A. Guimarães, "Spectrum sensing: A tutorial," *Journal of Communication and Information Systems*, vol. 37, no. 1, pp. 10–29, Feb. 2022, doi: 10.14209/jcis.2022.2.

[2] Federal Communications Commission, FCC, *Spectrum Policy Task Force Report*. FCC, 2002. [Online]. Available: https://books.google.com.br/books?id=p9MQtwAACAAJ.

[3] The Institute of Electrical and Electronic Engineers, IEEE, "IEEE 802 Part 22: Cognitive Wireless RAN Medium Access Control (MAC) and Physical Layer (PHY) Specifications: Policies and Procedures for Operation in the TV Bands," 2011. [Online]. Available: http://standards.ieee.org/getieee802/download/802.22-2011.pdf.

[4] T. Shongwe, A. J. H. Vinck, and H. C. Ferreira, "A study on impulse noise and its models," *SAIEE Africa Research Journal*, vol. 106, no. 3, pp. 119–131, 2015, doi: 10.23919/SAIEE.2015.8531938.

[5] D. A. Reynolds *et al.*, "Gaussian mixture models," *Encyclopedia of biometrics*, vol. 741, no. 659-663, 2009, doi: 10.1007/978-1-4899-7488-4-196.

[6] M. Shao and C. Nikias, "Signal processing with fractional lower order moments: stable processes and their applications," *Proceedings of the IEEE*, vol. 81, no. 7, pp. 986–1010, 1993, doi: 10.1109/5.231338.

[7] N. I. Miridakis, T. A. Tsiftsis, and G. Yang, "Moment-based spectrum sensing under generalized noise channels," *IEEE Communications Letters*, vol. 25, no. 1, pp. 89–93, 2021, doi: 10.1109/LCOMM.2020.3023740.

[8] L. Clavier, G. Peters, F. Septier, and I. Nevat, "Impulsive noise modeling and robust receiver design," *EURASIP Journal on Wireless Communications and Networking*, pp. 13–42, Jan. 2021, doi: 10.1186/s13638-020-01868-1.

[9] D. Middleton, "Statistical-physical models of electromagnetic interference," *IEEE Transactions on Electromagnetic Compatibility*, vol. EMC-19, no. 3, pp. 106–127, 1977, doi: 10.1109/TEMC.1977.303527.

[10] M. Liu, N. Zhao, J. Li, and V. C. M. Leung, "Spectrum sensing based on maximum generalized correntropy under symmetric alpha stable noise," *IEEE Transactions on Vehicular Technology*, vol. 68, no. 10, pp. 10 262–10 266, 2019, doi: 10.1109/TVT.2019.2931949.

[11] L. d. S. Costa and R. A. A. de Souza, "Performance of blind cooperative spectrum sensing under impulsive noise," in *2020 IEEE Latin-American Conference on Communications (LATINCOM)*, 2020, pp. 1–6, doi: 10.1109/LATINCOM50620.2020.9282340.

[12] A. Mehrabian, M. Sabbaghian, and H. Yanikomeroglu, "Spectrum sensing for symmetric α-stable noise model with convolutional neural networks," *IEEE Transactions on Communications*, vol. 69, no. 8, pp. 5121–5135, 2021, doi: 10.1109/TCOMM.2021.3070892.

[13] L. G. B. Guedes and D. A. Guimarães, "Direct-conversion spectrum sensor impaired by symmetric α-stable and α-sub-gaussian noises," *Journal of Communication and Information Systems*, vol. 38, no. 1, pp. 34–46, Feb. 2023, doi: 10.14209/jcis.2023.5. [Online]. Available: https://jcis.sbrt.org.br/jcis/article/view/852

[14] A. Mahmood and M. Chitre, "Modeling colored impulsive noise by Markov chains and alpha-stable processes," in *OCEANS 2015 - Genova*, 2015, pp. 1–7, doi: 10.1109/OCEANS-Genova.2015.7271550.

[15] ——, "Optimal and near-optimal detection in bursty impulsive noise," *IEEE Journal of Oceanic Engineering*, vol. 42, no. 3, pp. 639–653, 2017, doi: 10.1109/JOE.2016.2603790.

[16] M. Kanefsky and J. Thomas, "On polarity detection schemes with non-gaussian inputs," *Journal of the Franklin Institute*, vol. 280, no. 2, pp. 120–138, 1965, doi: 10.1016/0016-0032(65)90398-4. [Online]. Available: https://www.sciencedirect.com/science/article/pii/0016003265903984

[17] F. Moghimi, A. Nasri, and R. Schober, "Lp-norm spectrum sensing for cognitive radio networks impaired by non-gaussian noise," in *GLOBECOM 2009 - 2009 IEEE Global Telecommunications Conference*, 2009, pp. 1–6, doi: 10.1109/GLOCOM.2009.5425992.

[18] S. Kotz, T. Kozubowski, and K. Podgorski, *The Laplace Distribution and Generalizations: A Revisit with Applications to Communications, Economics, Engineering, and Finance*, ser. Progress in Mathematics. Birkhäuser Boston, 2001. [Online]. Available: https://books.google.com.br/books?id=cb8B07hwULUC

[19] N. C. Beaulieu and D. J. Young, "Designing time-hopping ultra-wide bandwidth receivers for multiuser interference environments," *Proceedings of the IEEE*, vol. 97, no. 2, pp. 255–284, 2009, doi: 10.1109/JPROC.2008.2008782.

[20] N. C. Beaulieu and S. Niranjayan, "UWB receiver designs based on a gaussian-laplacian noise-plus-mai model," *IEEE Transactions on Communications*, vol. 58, no. 3, pp. 997–1006, 2010, doi: 10.1109/TCOMM.2010.03.070333.

[21] F. Tan, X. Song, C. Leung, and J. Cheng, "Collaborative spectrum sensing in a cognitive radio system with laplacian noise," *IEEE Communications Letters*, vol. 16, no. 10, pp. 1691–1694, 2012, doi: 10.1109/LCOMM.2012.080312.120517.

[22] Y. Ye, Y. Li, G. Lu, and F. Zhou, "Improved energy detection with laplacian noise in cognitive radio," *IEEE Systems Journal*, vol. 13, no. 1, pp. 18–29, 2019, doi: 10.1109/JSYST.2017.2759222.

[23] Y. Ye, Y. Li, G. Lu, F. Zhou, and H. Zhang, "Performance of spectrum sensing based on absolute value cumulation in laplacian noise," in *2017 IEEE 86th Vehicular Technology Conference (VTC-Fall)*, 2017, pp. 1–5, doi: 10.1109/VTCFall.2017.8287978.

[24] K. Sinha and Y. N. Trivedi, "Cooperative spectrum sensing with hard decision fusion based on modified correlation detection scheme in additive laplacian noise," in *2022 3rd International Conference on Smart Electronics and Communication (ICOSEC)*, 2022, pp. 1–7, doi: 10.1109/ICOSEC54921.2022.9952119.

[25] H. Urkowitz, "Energy detection of unknown deterministic signals," *Proceedings of the IEEE*, vol. 55, no. 4, pp. 523–531, 1967, doi: 10.1109/PROC.1967.5573.

[26] R. Gao, Z. Li, H. Li, and B. Ai, "Absolute value cumulating based spectrum sensing with Laplacian noise in cognitive radio networks," *Wireless Personal Communications*, vol. 83, July 2015, doi: 10.1007/s11277-015-2457-4.

[27] H. Qu, X. Xu, J. Zhao, F. Yan, and W. Wang, "A robust hyperbolic tangent-based energy detector with Gaussian and non-Gaussian noise environments in cognitive radio system," *IEEE Systems Journal*, vol. 14, no. 3, pp. 3161–3172, 2020, doi: 10.1109/JSYST.2019.2959045.

[28] D. A. Guimarães, "Robust test statistic for cooperative spectrum sensing based on the Gerschgorin circle theorem," *IEEE Access*, vol. 6, pp. 2445–2456, 2018, doi: 10.1109/ACCESS.2017.2783443.

[29] ——, "Gini index inspired robust detector for spectrum sensing over ricean channels," *Electronics Letters*, Nov. 2018, doi: 10.1049/el.2018.7375.

[30] ——, "Pietra-Ricci index detector for centralized data fusion cooperative spectrum sensing," *IEEE Transactions on Vehicular Technology*, vol. 69, no. 10, pp. 12 354–12 358, 2020, doi: 10.1109/TVT.2020.3009440.

[31] D. Ramirez, J. Via, I. Santamaria, and L. L. Scharf, "Locally most powerful invariant tests for correlation and sphericity of gaussian vectors," *IEEE transactions on information theory*, vol. 59, no. 4, pp. 2128–2141, 2013, doi: 10.1109/TIT.2012.2232705.

[32] L. Huang, Y. Xiao, H. C. So, and J. Fang, "Accurate performance analysis of hadamard ratio test for robust spectrum sensing," *IEEE Transactions on Wireless Communications*, vol. 14, no. 2, pp. 750–758, 2015, doi: 10.1109/TWC.2014.2359223.

[33] L. Huang, C. Qian, Y. Xiao, and Q. T. Zhang, "Performance analysis of volume-based spectrum sensing for cognitive radio," *IEEE Transactions on Wireless Communications*, vol. 14, no. 1, pp. 317–330, 2015, doi: 10.1109/TWC.2014.2345660.

[34] B. Nadler, F. Penna, and R. Garello, "Performance of eigenvalue-based signal detectors with known and unknown noise level," in *2011 IEEE International Conference on Communications (ICC)*, 2011, pp. 1–5, doi: 10.1109/icc.2011.5963473.

[35] R. Zhang, T. J. Lim, Y.-C. Liang, and Y. Zeng, "Multi-antenna based spectrum sensing for cognitive radios: A GLRT approach," *IEEE Transactions on Communications*, vol. 58, no. 1, pp. 84–88, 2010, doi: 10.1109/TCOMM.2010.01.080158.

[36] T. Rappaport, *Wireless Communications: Principles And Practice, 2/E*. Pearson Education, 2010, isbn: 9788131731864. [Online]. Available: https://books.google.com.br/books?id=VmPT8B-5_tAC

[37] S. Zhu, T. S. Ghazaany, S. M. R. Jones, R. A. Abd-Alhameed, J. M. Noras, T. Van Buren, J. Wilson, T. Suggett, and S. Marker, "Probability distribution of rician k-factor in urban, suburban and rural areas using real-world captured data," *IEEE Transactions on Antennas and Propagation*, vol. 62, no. 7, pp. 3835–3839, 2014, doi: 10.1109/TAP.2014.2318072.

[38] D. A. Guimarães, "Modified Gini index detector for cooperative spectrum sensing over line-of-sight channels," *Sensors*, vol. 23, no. 12, 2023, doi: 10.3390/s23125403. [Online]. Available: https://www.mdpi.com/1424-8220/23/12/5403

[39] D. A. Guimarães and E. J. T. Pereira, "Influence of a direct-conversion receiver model on the performance of detectors for spectrum sensing," *Journal of Communication and Information Systems*, vol. 36, no. 1, p. 173–183, Nov. 2021, doi: 10.14209/jcis.2021.19.

[40] R. G. Newcombe, "Two-sided confidence intervals for the single proportion: comparison of seven methods," *Statistics in Medicine*, vol. 17, no. 8, pp. 857–872, 1998, doi: 10.1002/(SICI)1097-0258(19980430)17:8<857::AID-SIM777>3.0.CO;2-E.

[41] D. A. Guimarães and L. G. B. Guedes, "Matlab code for performance analysis of detectors for spectrum sensing under Laplacian noise," Dec. 2023. [Online]. Available: https://www.dropbox.com/scl/fi/h2gfuc2igdnmvtk7qe8fg/DetectorsLaplacianNoise.m?rlkey=4dpzztfughdmkyiceucr55e59&dl=0

[42] T. Eltoft, T. Kim, and T.-W. Lee, "On the multivariate laplace distribution," *IEEE Signal Processing Letters*, vol. 13, no. 5, pp. 300–303, 2006, doi: 10.1109/LSP.2006.870353.

[43] D. Wang, C. Zhang, and X. Zhao, "Multivariate laplace filter: A heavy-tailed model for target tracking," in *2008 19th International Conference on Pattern Recognition*, 2008, pp. 1–4, doi: 10.1109/ICPR.2008.4761002.

Luiz Gustavo Barros Guedes received the BSc (2019) and the MSc (2023) degrees in Telecommunications Engineering from the National Institute of Telecommunications (Inatel), Brazil. He is working towards the PhD degree and works as a Researcher at Inatel. His research interests are digital transmission, signal processing, mobile communications, dynamic spectrum access, probability and statistics.

Dayan Adionel Guimarães received the MSc (1998) and the PhD (2003) degrees in Electrical Engineering from the State University of Campinas (Unicamp), Brazil. He is a Researcher and Senior Lecturer with the National Institute of Telecommunications (Inatel), Brazil. His research interests are the general aspects of wireless communications, specifically radio propagation, digital transmission, dynamic spectrum access and signal processing applied to telecommunications.